Atmospheric Environment xxx (xxxx) xxx

Contents lists available at ScienceDirect

Atmospheric Environment

journal homepage: http://www.elsevier.com/locate/atmosenv

Temporal and spatial variations of aerosol optical properties over the Korean peninsula during KORUS-AQ

Yongjoo Choi [a,1,*], Young Sung Ghim [a], Michal Segal Rozenhaimer [b,c,d], Jens Redemann [e], Samuel E. LeBlanc [b,c], Connor J. Flynn [e], Roy J. Johnson [b], Yonghwan Lee [a], Taehyoung Lee [a], Taehyun Park [a], Joshua P. Schwarz [f], Kara D. Lamb [f,g], Anne E. Perring [f,g,2]

[a] Department of Environmental Science, Hankuk University of Foreign Studies, 17035, South Korea
[b] NASA Ames Research Center – Moffett Field, CA, USA
[c] Bay Area Environmental Research Institute – Moffett Field, CA, USA
[d] Department of Geophysics, Porter School of the Environment and Earth Sciences, Tel-Aviv University, Tel-Aviv, Israel
[e] University of Oklahoma – Norman, OK, USA
[f] Chemical Sciences Division, NOAA Earth System Research Laboratory, Boulder, CO, USA
[g] Cooperative Institute for Research in the Environmental Sciences, University of Colorado Boulder, Boulder, CO, USA

HIGHLIGHTS

- Investigation of temporal/spatial variations in aerosol optical properties during KORUS-AQ.
- Homogeneous spatial distribution of fine mode aerosols in the west-to-east direction.
- Active secondary formation in the downwind region of Seoul.

ARTICLE INFO

Keywords:
KORUS-AQ
AERONET
DC-8
Aerosol optical and chemical properties
Secondary aerosol formation

ABSTRACT

We investigated the temporal and spatial variations of aerosol optical properties over the Korean peninsula during the KORUS-AQ (KORea–United States Air Quality) experiment with ground-based aerosol optical properties measured by remote and *in-situ* techniques. On the ground, AErosol RObotic NETwork (AERONET) and ground-level particulate matter (PM) concentration from air quality monitoring stations were used. From the NASA DC-8 research aircraft, the airborne Spectrometer for Sky-Scanning, Sun-Tracking Atmospheric Research instrument (4STAR), an aerosol mass spectrometer (AMS), and a single particle soot photometer (SP2) provided aerosol information. Average hourly fine- and coarse-mode aerosol optical depth (AOD) and fine mode fraction (FMF), were divided into four clusters (background, Seoul Metropolitan Area (SMA), southwest, and east) representing different temporal/spatial variations; the results of those clusters were similar to the clustering results using PM from air quality monitoring stations. The downwind region of SMA was dominant by light-scattering fine-mode aerosols likely due to secondary aerosol formation with high fine-mode AOD and single scattering albedo compared to other regions, even Seoul. The fine-mode aerosols were more spatially homogeneous than coarse-mode aerosols, especially in the west-to-east direction, because fine-mode aerosols are usually transported on a regional scale by westerlies rather than emitted from local emission sources. However, the aerosol size distribution was spatially more homogeneous because of a consistent contribution of fine- and coarse-mode AOD to total AOD regardless of direction between the AERONET sites. During high-aerosol loading episodes, the temporal and spatial variations of aerosol optical properties were similar to those derived from 4STAR and ground-level PM concentrations, providing detailed information on aerosol behavior and characteristics. Using missed-approach flight segments (touchdown and take-off without a full-stop), investigation of diurnal variations over the SMA revealed a significant increase in AOD and Angstrom exponent (AE) in the afternoon compared to morning and noon, especially in the downwind region, because of more active secondary formation resulting

* Corresponding author. Research Institute for Global Change, Japan Agency for Marine-Earth Science and Technology, Yokohama, Japan.
E-mail address: choingjoo@jamstec.go.jp (Y. Choi).
[1] Now at Research Institute for Global Change, Japan Agency for Marine-Earth Science and Technology, Yokohama, Japan.
[2] Now at Department of Chemistry, Colgate University, Hamilton, NY, USA.

https://doi.org/10.1016/j.atmosenv.2021.118301
Received 6 August 2020; Received in revised form 13 January 2021; Accepted 26 February 2021
Available online 2 March 2021

from advected and/or emitted local pollutants and precursors. The diurnal variation of PM_1 in the downwind region was similar to that of AOD; it was mainly increased during the day by secondary organic aerosols and ammonium nitrate due to large amounts of isoprene and meteorological conditions that supported secondary aerosol formation. Ammonium sulfate also partially led to increasing the PM_1, but its behavior was unclear, because RH decreased during the day, which would imply the reduced aqueous-phase oxidation (the major pathway for sulfate production). Compared to the downwind region, ammonium nitrate and refractory black carbon decreased in Seoul because of a slightly decreased traffic volume, dissociation of ammonium nitrate, and increased boundary layer height according to meteorological conditions in the afternoon. The results of this study provide detailed information on aerosol behavior given the synergy of the various measurement platforms used. Along with the evidence of active photochemical reactions taking place in the downwind region, such data will be useful in formulating policies that improve air quality in Korea.

1. Introduction

Aerosols can reduce the visibility and damage human health on a local scale, affect air quality on a regional scale, and affect climate change directly by absorbing and scattering solar radiation, and indirectly by altering cloud properties on a global scale (Myhre et al., 2013; Pope and Dockery, 2006; WHO, 2006). East Asia underwent dramatic growth in its economy and energy production in the several decades leading up to 2010, accompanied by an increase in pollutant emissions. Although rigid strategies for emission control were implemented to improve human health (Zheng et al., 2018), East Asia is still the largest area for pollution emissions (Crippa et al., 2018; Kurokawa and Ohara, 2020). In particular, the air quality of the Seoul Metropolitan Area (SMA) is important, because the population of the SMA is ~25 million, which is approximately half of the total Korean population. Although fine-mode aerosols have become a major societal issue in Korea over the past few years along with increased public attention (Ghim et al., 2017), it is difficult to control the air quality in Korea due to the combination of both primary and secondary aerosol pollution from local sources and long-range transported ones (Ghim et al., 2019; Jordan et al., 2020; Peterson et al., 2019), and because aerosols are highly influenced by not only the atmospheric chemical process, but also meteorological factors (Seinfeld and Pandis, 2016).

To monitor the relative importance of long-range transported and/or local pollutants along with their chemical compositions, several air quality monitoring stations have been installed in key places. However, operating and maintaining of those stations is labor-intensive and costly. Therefore, ground-based aerosol optical networks, which were initially installed to verify satellite-based observations, are now widely used for air quality monitoring as an alternative and an auxiliary proxy for ground-truth, because the measurement period has been extended to over 20 years and because the data are easily acquired. Among those networks, the AErosol RObotic NETwork (AERONET; Holben et al., 1998), which consists of more than 550 sites worldwide, is widely used to analyze aerosol optical properties by means of standardized retrieval processing and instrument management. Furthermore, because of improvements in retrieval algorithms and data accuracy (Giles et al., 2019; Sinyuk et al., 2020), the scope of research has been expanded to include not only investigation of the aerosol optical properties but also estimation of the dominant aerosol types, broadly representing an underlying chemical composition and/or mass concentration of those aerosols (Choi and Ghim, 2016; Choi et al., 2016, 2020; Li et al., 2019; Russell et al., 2014; Schuster et al., 2016a, 2016b; Zhang et al., 2018).

To increase our understanding of the factors contributing to poor air quality in Korea, the KORUS-AQ campaign, an intensive intercontinental cooperative air quality field study, was conducted from May to June 2016 (Al-Saadi et al., 2015). The campaign involved numerous measurement sites and platforms, including ground-based (Bae et al., 2017; Kim et al., 2018; Park et al., 2018), ship-borne, and airborne measurements (Jeong et al., 2019; Lamb et al., 2018; Nault et al., 2018) with the overarching goals of validating satellite retrievals (Choi et al., 2019b), chemical transport models (Choi et al., 2019a; Ha et al., 2020; Huang et al., 2018; Lennartson et al., 2018), and emission inventories (Goldberg et al., 2019; Miyazaki et al., 2019). In addition, AERONET Cimel sunphotometers were deployed at about 20 sites over Korea, including the SMA and rural/background areas, as part of the Distributed Regional Aerosol Gridded Observation Networks (DRAGONs) deployment (Holben et al., 2018). However, there is still a lack of approaches that consider the temporal and/or spatial variation analysis as an aspect of aerosol optical and chemical properties using the ground-based measurement data.

This study focuses on spatial and temporal variations in aerosol optical properties measured from the AERONET sites augmented by research flights of the NASA DC-8, which deployed the Spectrometer for Sky-Scanning, Sun-Tracking Atmospheric Research (4STAR) to elucidate variations between ground-based monitoring sites in terms of aerosol optical and chemical properties. Using cluster analysis, we examined the characteristics of aerosol optical properties for each AERONET cluster in order to assess the geographical characteristics. Next, we investigated the characteristics of spatial variation using the relationship between correlation coefficients (R) of aerosol optical properties from different AERONET sites as a function of site distance. Then, the spatial and temporal variations of aerosol optical properties during the selected episodes were investigated along with those from 4STAR and particulate matter (PM) concentrations from air quality monitoring stations. Finally, we investigated the diurnal variation in aerosol optical properties measured from 4STAR over the SMA using missed-approach flight segments (i.e., missed aircraft approaches).

2. Methods

2.1. AErosol RObotic NETwork (AERONET)

Cimel sunphotometers (CE 318) were installed at 20 sites including urban, rural, and background regions over the Korean Peninsula during the KORUS-AQ campaign, mainly focused on the SMA (Table 1 and Fig. 1). CE 318 was measured at several wavelengths, typically centered at 0.34, 0.38, 0.44, 0.50, 0.67, 0.87, 0.94, and 1.02 μm (e.g., Holben et al., 1998; Holben et al., 2001). All of these spectral bands are utilized in the direct sun measurements, whereas only four of them (0.44, 0.67, 0.87, and 1.02 μm) are used for the sky radiance measurements. Spectral aerosol optical depth (AOD) is obtained from direct sun measurements with high accuracy (±0.01 to 0.02) (Eck et al., 1999). Other aerosol optical properties, such as single scattering albedo (SSA) and volume size distribution, are retrieved from an inversion of combined sky radiance and AOD measurements (Dubovik et al., 2000, 2006). We used recently developed version 3 AERONET level 2 products which passed an improved cloud screening process and were quality assured by applying post-field calibration (Giles et al., 2019; Sinyuk et al., 2020). It should be noted that version 3 products allow a high level of fluctuation in fine-mode aerosols; these are reported as aerosols; a misidentification as clouds, as in the version 2 dataset, is thereby diminished from the current dataset. In this study, we used fine- and coarse-mode AOD at 500 nm obtained from a spectral deconvolution algorithm (SDA) product (Arola et al., 2017; O'Neill et al., 2001; O'Neill et al., 2003), and SSA at 440 nm from the inversion product. In addition to the fine mode

fraction (FMF), the ratio of fine-mode AOD to total AOD, was used as an aerosol size parameter. However, the level 2 criterion of AOD at 440 nm (AOD_{440}) $\geq$ 0.4 for SSA is often too strict, considering that AOD_{440} is smaller than 0.4 at many sites. Therefore, we used a lower AOD_{440} threshold of 0.2 by replacing the inversion products from level 1.5 (cloud screened data) for 0.2 $\leq$ AOD_{440} < 0.4, which passed other quality-assured level 2 criteria (Arola et al., 2015; Choi and Ghim, 2016; Choi et al., 2020), because the mean error between the retrieval and measurement values of the SSA is about 1% when AOD $\geq$ 0.2 (Dubovik et al., 2000).

2.2. DC-8 research flights and 4STAR

The NASA DC-8 flew 20 research flights (RFs) to geographically cover the Korean peninsula, Yellow Sea, and East China Sea (Fig. 1b). For each RF, the DC-8 took off from the Osan air base, approximately 60 km south of Seoul city hall, typically at 08:00 local time (LT), and conducted a missed-approach at Seoul Air Base (Seongnam), which is located about 15 km south of Seoul city hall. The missed-approaches were typically performed two more times per flight for a total of three approaches: after take-off around ~09:00 LT, around noon, and prior to landing (~16:00 LT), by sequentially overpassing the upwind (Namyangju and Guri), Seoul (Songpa - Olympic Park and Gangnam), and downwind regions (Seongnam, Gwangju - Teahwa Forest, Icheon, and Yeoju). These repeated flight patterns are suitable for providing statistical data on the diurnal variation in aerosol information over the SMA, including upwind and downwind regions.

During the research flight, AOD and Angstrom exponent (AE) were measured by 4STAR operating in sun-tracking mode. Trace gas retrievals (Segal-Rosenheimer et al., 2014) are also available observations in the sun-tracking mode, but here we focused on the properties of aerosols. Because a detailed description of the instrument's technical features, validation, and retrieval process can be found elsewhere (Dunagan et al., 2013; Segal-Rosenheimer et al., 2013; Shinozuka et al., 2013), we only briefly describe it here. The optical head of the 4STAR is installed on top of the DC-8 fuselage. 4STAR has two grating array spectrometers that cover the UV-SWIR (UV-VIS-NIR, 210–995 nm and SWIR, 950–1703 nm), which are combined to yield continuous spectra. The spectral resolution is 2–3 nm below 1000 nm and 3–7 nm at longer wavelengths, and the full-width field of view (FOV) is 2.4° when making direct sun measurements (LeBlanc et al., 2020). We used the AOD at 501 nm and AE from 441 to 871 nm with a 1 s measurement interval. The reported uncertainty in spectral AOD is estimated as order 0.005–0.02, which decreases with increasing wavelength (Sayer et al., 2019).

2.3. Ancillary data

To compare the aerosol optical properties with ground-level PM, we used PM_{10} and $PM_{2.5}$ mass concentrations measured from 211 sites of nationwide air quality monitoring stations operated by the National Institute of Environmental Research (NIER) on the Korean peninsula (Fig. S1). PM mass concentration was measured using a FH 62 C14 Continuous Particulate Monitor (Thermo Scientific). The instrument is operated by the principle of beta-ray attenuation by means of particles collected on a movable filter tape. The measuring position is continuously fed with a new section of filter tape. Ambient air is pulled through the inlet and sample tube to induce the deposition of particles on the filter, through which the beta-ray passes. The intensity of the beta-ray, expressed as the count rate from the detector, is inversely proportional to the particle mass loaded on the filter. The minimum detection limit for PM_{10} is < 1 μg m^{-3} with a precision of ±2 μg m^{-3} (Choi and Ghim, 2017). We matched similar characteristics between the AERONET and PM data to compare representative column aerosols with ground-level PM despite the inherent differences between AERONET and PM data. For example, fine- and coarse-mode aerosols correspond to $PM_{2.5}$ and $PM_{10\text{-}2.5}$ (the difference between PM_{10} and $PM_{2.5}$). $PM_{2.5}/PM_{10}$ was also calculated from the ratio between $PM_{2.5}$ and PM_{10} to identify aerosol size and enable comparisons with FMF from AERONET.

2.4. Cluster analysis of aerosol optical properties from AERONET

To distinguish between groups with similar temporal variations in aerosols, a cluster analysis was conducted using aerosol optical properties from AERONET. First, we used hourly average fine-mode AOD, coarse-mode AOD, and FMF from Level 3 SDA products at each site. Second, the AERONET sites were distinguished using a hierarchical clustering function (https://stat.ethz.ch/R-manual/R-devel/library/stats/html/hclust.html), included in the standard R package, "stats" with the option of Ward's method ('ward.D2') for linkage with Euclidean distances for dissimilarity metric. Because the hierarchical methods did

Table 1
Detailed information on the 20 AERONET sites used in this study.

No.[a]	Site name	Longitude (° E)	Latitude (° N)	Elevation (m)	Type
	Background				
1	Baengnyeong	124.63	37.97	136	Background
2	Socheongcho	124.74	37.42	28	Background
	SMA				
3	KORUS_NIER	126.64	37.57	26.9	Urban
4	Yonsei_University	126.93	37.56	88	Urban
5	Seoul_SNU	126.95	37.46	116	Urban
6	KORUS_Olympic_Park	127.12	37.52	45	Urban
7	Hankuk_UFS	127.27	37.34	167	Rural
8	KORUS_Taehwa	127.31	37.31	152	Rural
9	KORUS_Songchon	127.49	37.34	90	Rural
10	KORUS_Baeksa	127.57	37.41	64	Rural
	Southwest				
11	Anmyon	126.33	36.54	47	Rural
12	KORUS_Iksan	127.01	35.96	84	Urban
13	Gwangju_GIST	126.84	35.23	52	Urban
14	KORUS_Mokpo_NU	126.44	34.91	26	Urban
15	Gosan_SNU	126.16	33.29	72	Background
	East				
16	Gangneung_WNU	128.87	37.77	60	Urban
17	KORUS_Daegwallyeong	128.76	37.69	837	Background
18	KORUS_Kyungpook_NU	128.61	35.89	65	Urban
19	KORUS_UNIST_Ulsan	129.19	35.58	106	Urban
20	Pusan_NU	129.08	35.24	71	Urban

[a] Numbers in Fig. 1a.

not provide the optimal number of clusters, we chose the optimal number of groups by comparing the reasonableness of the spatial division pattern of each cluster when the number of clusters was increased. The AERONET sites were classified as 'SMA' and 'other' when the number of clusters was two. As the number of clusters increased to three, 'other' was divided into 'southwest' and 'other.' When the number of clusters was four, 'other' was further divided into 'background' and 'east' regions. Because the 'southwest' cluster was divided into a northern part and a southern part when the number of clusters was increased to five, we decided that four was the optimal number of clusters to represent the homogeneous/heterogeneous spatial distribution in Korea during the KORUS-AQ campaign. The uncertainties from the different selecting dissimilarity metrics (Manhattan and Minkowski distances) and/or linkage methods (average and complete linkages) are believed to be negligible because the pattern of distinguished clusters was exactly the same as the original one, or only 'Gosan' was separated from the southwest cluster alone. As shown in Fig. 1a, the geographical location of each group was well divided by latitude and distance from China.

We also did cluster analysis using nationwide PM air quality monitoring stations to verify and compare the results from AERONET; the results were similar to those from AERONET and divided Korea into 'SMA,' 'west,' 'southwest,' and 'east' (Fig. S1). In addition, the variations in $PM_{2.5}$ and PM_{10} mass concentration and $PM_{2.5}/PM_{10}$ were similar to the temporal and spatial variations of AERONET, confirming that cluster analysis using AERONET could represent ground-level PM variation.

3. Results and discussion

3.1. Aerosol optical properties of clusters

Fig. 2 shows the averaged aerosol optical properties from 20 AERONET sites with an overall average for each cluster during the KORUS-AQ campaign. SSA is the ratio of scattering efficiency to total extinction efficiency. SSA is high for most aerosols because they effectively scatter light, but is particularly high for fine-mode aerosols without carbonaceous materials, such as secondary inorganic ions (SII), comprised of ammonium sulfate and nitrate. We used FMF for the aerosol size parameter instead of the more traditional choice of AE because AE does not provide clear information in the intermediate range between 1 and 2, which occurs frequently for atmospheric aerosols (Prats et al., 2011; Schuster et al., 2006). AAOD is absorption AOD, calculated by multiplying AOD by (1–SSA) at 440 nm, which represents light-absorbing aerosols.

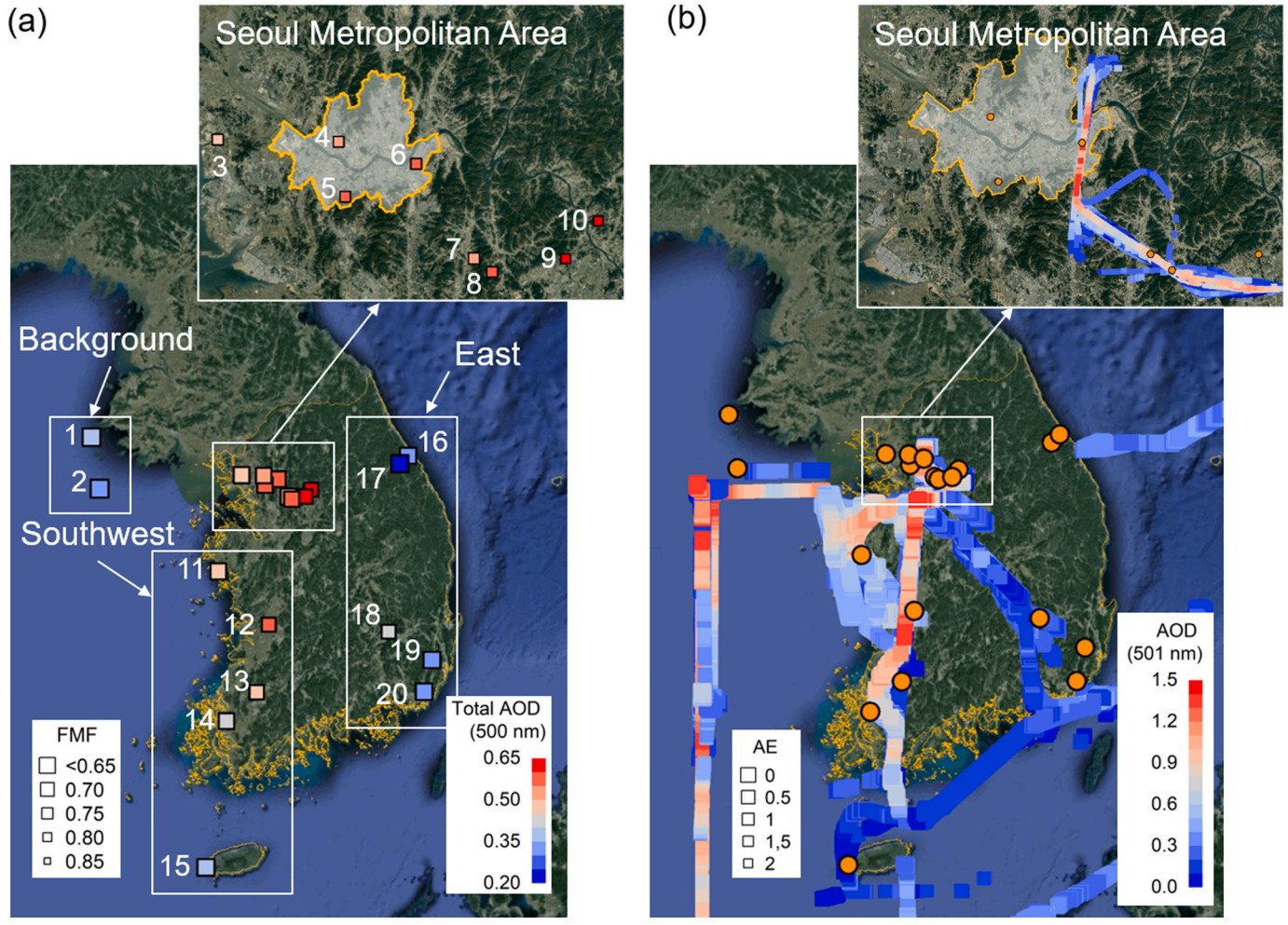

Fig. 1. (a) Location of AERONET sites during the KORUS-AQ campaign. The color and size of the symbols indicate the mean total aerosol optical depth (AOD) and fine mode fraction (FMF; ratio of fine mode AOD to total AOD) at 500 nm calculated with version 3 spectral deconvolution algorithm (SDA) level 2 products. The four white boxes indicate the geographical location of the four clusters, which were separated by cluster analysis using average hourly fine- and coarse-mode AOD and FMF from AERONET data. Detailed information on AERONET sites is summarized in Table 1, with the corresponding numbers beside the symbols. (b) Mean AOD at 501 nm and AE between 441 nm and 871 nm from 4STAR on board the NASA DC-8 along with the research flight track when the flight altitude was less than 1 km. The inset in Fig. 1b depicts the missed approach over the Seoul Metropolitan Area (SMA). The orange circles indicate AERONET sites. (For interpretation of the references to color in this figure legend, the reader is referred to the Web version of this article.)

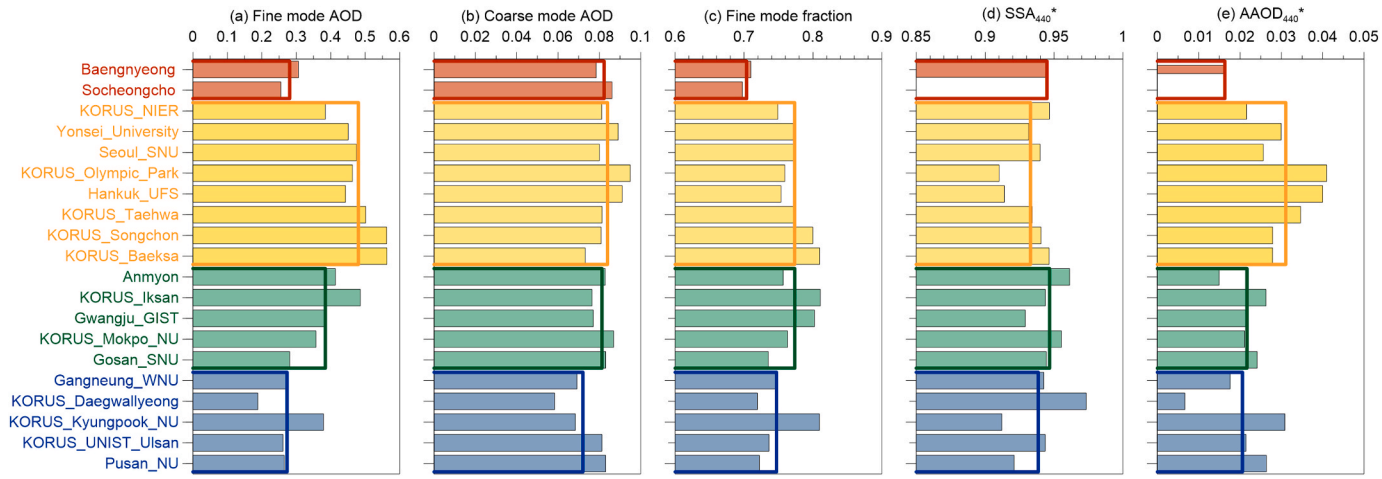

Fig. 2. Mean aerosol optical properties from 20 AERONET sites (bar plots) and overall mean of each cluster (non-filled bar plots) during the KORUS-AQ campaign. The filled and non-filled red, yellow, green, and blue color bars indicated 'background', 'Seoul Metropolitan Area', 'southwest' and 'east' cluster, respectively. (a) Fine-mode AOD, (b) coarse-mode AOD, (c) fine mode fraction from version 3 (V3) spectral deconvolution algorithm (SDA) level 2 products, (d) single scattering albedo, and (e) absorption AOD at 440 nm from V3 inversion products which applied the lower AOD threshold of ≥0.2 instead of the original threshold of ≥0.4. (For interpretation of the references to color in this figure legend, the reader is referred to the Web version of this article.)

The overall average (with standard deviation) fine-mode AOD, coarse-mode AOD, and FMF were 0.38 ± 0.11, 0.08 ± 0.01, and 0.76 ± 0.03, respectively. The average fine-mode AOD was highest in SMA, followed by southwest, east, and background, indicating that local emissions near SMA were higher than in other regions. Because fine-mode AOD did not significantly differ between the background and east regions (Student *t*-test $p > 0.1$), local emission and/or secondary formation may have been the main factor in deterioration of air quality in Korea during the KORUS-AQ campaign, rather than long-range transported pollutants. The fine-mode AOD in SMA gradually increased with increasing distance from Seoul, from 0.44 to 0.56 (Hankuk_UFS, KORUS_Taehwa, KORUS_Songchon, and KORUS_Baeksa) and fine-mode AOD in the downwind region was slightly higher than that in Seoul (Yonsei_University, Seoul_SNU, and KORUS_Olympic_Park). Moreover, FMF and SSA in the downwind region also gradually increased, from 0.75 to 0.81 and 0.91 to 0.95, respectively. This can be interpreted as an indication that the concentration of light-scattering fine-mode aerosols (such as ammonium nitrate and ammonium sulfate) increased due to secondary formation under high temperatures and low wind speed in the downwind region (Choi and Ghim, 2016; Lee et al., 2016) when we consider that the downwind region emitted less pollutants overall because of having less urbanization and a lower traffic volume. In contrast, AAOD was highest in KORUS_Olympic_Park and Hankuk_UFS, indicating that carbonaceous aerosols, such as black carbon (BC) and organic carbon (OC), were dominant.

The highest fine-mode AOD (except for that seen in SMA) was observed in KORUS-Iksan, which is located in southwest, the middle part of the west region; that value was 0.49. PM_{10} and $PM_{2.5}$ from PM monitoring stations co-located with AERONET also showed high concentrations, 67 and 36 μg m^{-3}, respectively, among all ~211 sites. Although Iksan is a small city with a population of about 30,700, KORUS-Iksan showed the highest fine-mode AOD because the National Industrial Complex is located near the measurement site (~2 km east). Cho and Song (2017) also reported that PM_{10} concentration at the same site was highest among all sites monitored in Jeollabuk-do province (southwestern part in Korea). By the same token, AAOD and FMF in KORUS-Iksan were relatively higher than the values in other regions, likely due to the high concentration of primary pollutants emitted from the National Industrial Complex.

The coarse-mode AOD was much lower than fine-mode AOD and did not show significant differences between clusters. There were fewer coarse particles during May and June, because of low wind speed and high relative humidity, which are the opposite conditions necessary for mineral dust occurrence (Choi et al., 2014). Therefore, FMF was much higher than 0.5 (low in the background region and high in the SMA) because fine-mode aerosols were a major factor for determining aerosol loading. The highest SSA with the lowest AOD was observed in KORUS-Daegwallyeong, which is located in a rural mountainous area (837 m asl) on the east coast of Korea, because there are no anthropogenic emission sources nearby. Therefore, this site represented the influence of maritime aerosols, which are known to have low AOD (≤0.2) and high SSA (≥0.95) (Quinn and Bates, 2005; Smirnov et al., 2002, 2011).

3.2. Relationship of correlation coefficient of aerosol optical properties to distances between AERONET sites

To investigate the degree of heterogeneity of the spatial distribution of aerosol optical properties, we examined the relationship of the correlation coefficient, *R*, for hourly average aerosol optical properties between two AERONET sites with the distance between the sites (Fig. 3). The overall median *R* among 190 pairs was 0.54 for both fine- and coarse-mode AOD and 0.58 for FMF. Among sites within the same cluster, the median *R* for fine-mode AOD (0.83), coarse-mode AOD (0.81), and FMF (0.87) showed better agreement than each overall median *R*, confirming much more homogeneous distributions within ~100 km. Generally, the relationship between *R* and the distance between two sites showed a strong negative trend with relatively high coefficients of determination (R^2), 0.72 for fine-mode AOD, 0.69 for coarse-mode AOD, and 0.46 for FMF. The different levels of R^2 indicate that the degree of heterogeneity of temporal variation of fine- and coarse-mode AOD and FMF can be determined by the distance between the sites. The slope of a linear least squares regression line between two variables (*R* and distance between sites) for coarse-mode AOD was lower (−0.14/100 km) than that for fine-mode AOD (−0.16/100 km), indicating that coarse particles were more spatially homogeneous. Because the variation in coarse-mode AODs in each cluster was constant compared to that of fine-mode AODs (Fig. 2). The slope of linear least squares regression line for FMF (−0.11/100 km) was the lowest, suggesting that the aerosol size distribution was the most spatially homogeneous as the result of a consistent contribution of fine- and coarse-mode AOD to total AOD despite fine-mode AOD showing more spatial variability (Lee and Son, 2016).

Within the same cluster, the R^2 for fine-mode AOD, coarse-mode

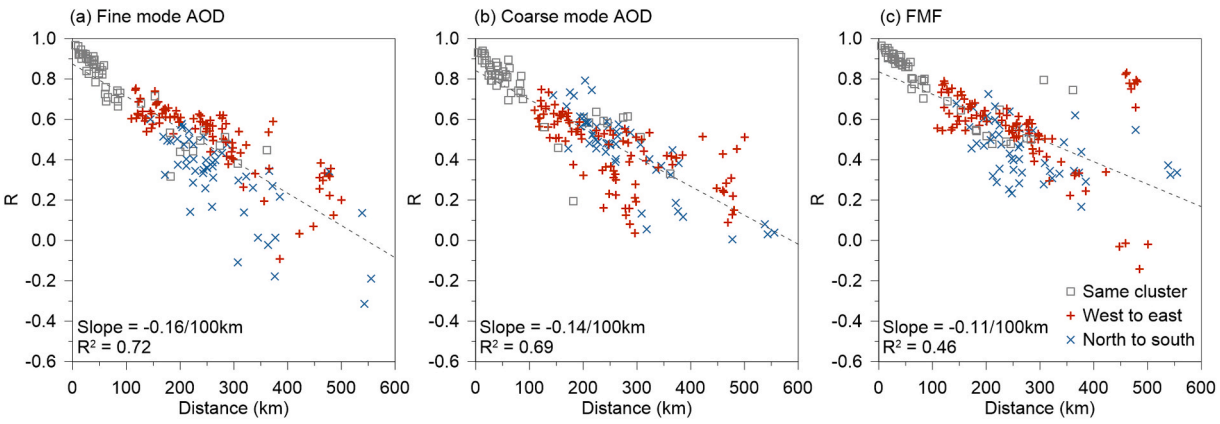

Fig. 3. Scatter plots of correlation coefficient (R) between hourly AERONET sites measurements and the distance between the AERONET sites for (a) fine-mode AOD, (b) coarse-mode AOD, and (c) fine-mode fraction (FMF). The colored symbols indicate the paired AERONET sites belonging to the same cluster or directions between two sites (west-to-east and north-to-south) within the different clusters.

AOD, and FMF were 0.84, 0.70, and 0.68, respectively. In addition, the slopes of linear least squares regression lines for fine-mode AOD and FMF within clusters were slightly steeper than those of overall cases (−0.18/100 km and −0.13/100 km, respectively), whereas that for coarse-mode AOD showed a similar range (−0.14/100 km). In contrast, the R^2 for fine- and coarse-mode AOD from the different clusters showed patterns that depended on the direction between the two sites; R^2 of the west-to-east direction (0.68 and 0.41, respectively) was lower than that of the north-to-south direction (0.78 and 0.79, respectively). The lower R^2 in the west-to-east direction likely results from not only the intensity and spatial extent of transported pollutants from the west to the east, but also the secondary formation at the local scale, which varied significantly by day. Indeed, the slope of the linear least squares regression lines for fine- and coarse-mode AOD in the west-to-east direction (−0.12/100 km and −0.10/100 km, respectively) were much lower than those of the north-to-south direction (−0.19/100 km and −0.17/100 km). In other words, the spatial distribution of aerosols in the west-to-east direction was less influenced by distance and was more homogeneous than that in the north-to-south direction, because the pollutants were mainly transported by the dominant westerlies. Coarse-mode aerosols were generally more spatially homogeneous regardless of direction compared to fine-mode aerosols. Lee and Son (2016) reported that fine aerosols were generally more spatially homogeneous compared to coarse particles, which were transported largely in the west-to-east direction, during the DRAGON-Asia campaign. However, because DRAGON-Asia was conducted in the spring, which is more influenced by mineral dust, the trend was opposite to that seen in this study.

3.3. Time series of aerosol optical properties during the KORUS-AQ campaign

It is hard to investigate the detailed temporal and spatial variations of aerosols, because AERONET sites have some spatial gaps. Therefore, we used information from the 4STAR installed on the DC-8 to cover those areas during the daytime. Before investigating the aerosol spatial distribution from 4STAR, we validated the representative AODs from 4STAR depending on flight altitude, because the altitude of the DC-8 could differ by up to 8 km depending on the purpose of the research flight. We compared AOD from 4STAR with AERONET, which measured within ±0.05° (longitude and latitude) and ±5 min based on AERONET site. The correlation coefficients and slope of a linear least squares regression line between 4STAR and AERONET AOD decreased as the altitude interval increased (Fig. 4). Although the root mean square deviation between two AODs ≤1.0 km altitude was slightly high at 0.14, possibly due to the near surface aerosol contribution not observed by 4STAR, the R^2 and slope of the linear least squares regression line were 0.80 and 0.78, respectively. Differences in full column AOD between the airborne 4STAR and ground-based AERONET have been shown to be smaller, with root-mean-square values of 0.01–0.03, depending on wavelength (LeBlanc et al., 2020; Shinozuka et al., 2013). The bias

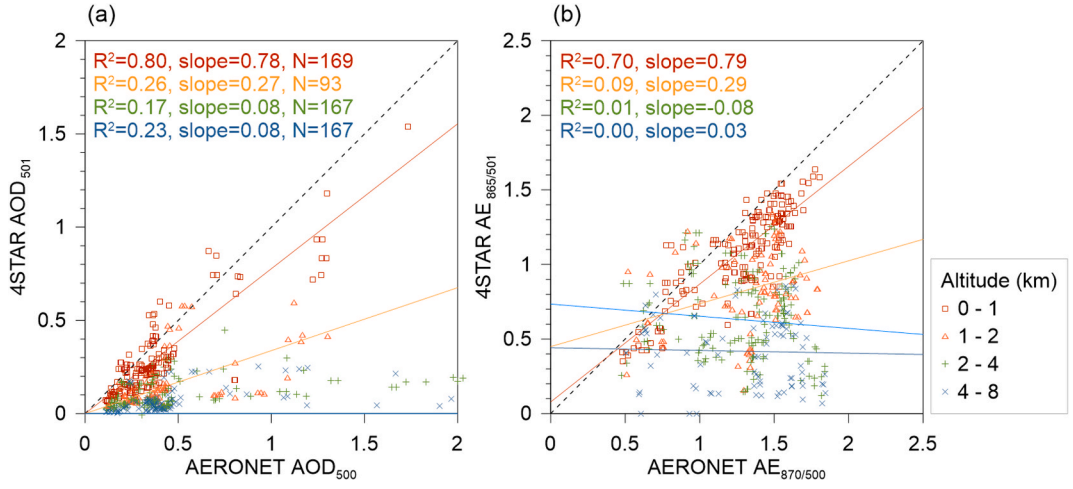

Fig. 4. Comparison of (a) AODs and (b) AEs between AERONET and 4STAR depending on altitude. The dashed line and colored lines indicate 1:1 line and linear least squares regression lines between two datasets corresponding to altitude, respectively.

between AOD from 4STAR measured at altitudes below 1 km and the ground-based AERONET in this case likely results from the contribution of aerosol below the aircraft during the time of measurement. The relationship of AE was similar to that of AOD. Therefore, we decided that AOD and AE from 4STAR taken at altitudes of less than 1 km adequately represent ground-based measurements. Of 20 total research flights, we excluded the three that were above 1 km.

Fig. 5 shows the time series of daily average aerosol optical properties for AERONET clusters during the KORUS-AQ campaign. There were distinct episodes resulting from significant large-scale meteorological variations, such as (1) 'Asian dust' from China and Mongolia (May 4 to 7), (2) 'local pollution' due to stagnant conditions (May 17 to 22), and (3) 'long-range transportation' from China (May 25 to 31) (Peterson et al., 2019). The transport pathways of airmass for those distinct episodes were also consistent with their properties (e.g., from Gobi desert on the Asian dust episode and from East China on the long-range transportation episode) (Fig. S3). The overall average AOD from 4STAR over Korea was 0.26, which is lower than that from AERONET (0.46), because the 4STAR covered rural regions in which the AERONET was not installed (Fig. 1b). It should be noted that the overall average 4STAR AOD does not represent temporal and/or spatial distribution of aerosols, because 4STAR measured AOD at the time and place along the aircraft path, whereas the distributed AERONET site measured semi-continuously over time, but only at their localized sites. Therefore, 4STAR accurately and widely captured the high AOD on the west coast of Korea and the Yellow Sea during the KORUS-AQ campaign according to flight purpose. In addition, it is worth noting that Jeollabuk-do showed relatively high AOD from AERONET (KORUS-Iksan) due to emissions from the chemical complex nearby. The highest AOD in Jeollabuk-do was also Jeonju, which is near Iksan, along with the highest PM_{10} and $PM_{2.5}$ concentrations (112 μg m^{-3} and 59.9 μg m^{-3}, respectively) during the KORUS-AQ campaign.

The temporal and spatial variations of aerosol optical properties differed according to the characteristics of high aerosol loading episodes. For example, the coarse-mode AOD rapidly increased during Asian dust transport episodes, especially on May 7, as announced by the Korea Meteorological Administration (KMA). The highest coarse-mode AOD in the western AERONET cluster agreed with the high $PM_{10\text{-}2.5}$ concentration in a similar region (southwest in Fig. S2). Low SSA and high AAOD were observed during Asian dust episodes, because not only iron oxide (e.g., goethite and hematite) but also carbonaceous aerosols might be mingled with mineral dust that contributed to light absorption (Kim et al., 2005; Linke et al., 2006; Schuster et al., 2016a). The dust aerosols were advected from China, reached the SMA at midnight, and peaked at 03:00 LT with a sudden increase in $PM_{10\text{-}2.5}$ concentration (Fig. 6). Then, the dust plume quickly passed through the SMA and moved toward the southwest, then onto the west region, where it peaked at 08:00 LT and 12:00 LT, respectively. Therefore, the AOD from AERONET first registered the dust as a high coarse-mode AOD in the west region in the early morning. In particular, the PM_{10} concentration and AOD in SMA were lower than those in other regions (Fig. 6g and h), as a large amount of mineral dust had already sunk or passed the surface level over time because of the high concentration in the south and east directions. It can also be deduced that mineral dust mainly existed at the surface level, at altitudes of less than 1 km, because 4STAR AOD was significantly smaller than AERONET AOD at its lowest altitudes.

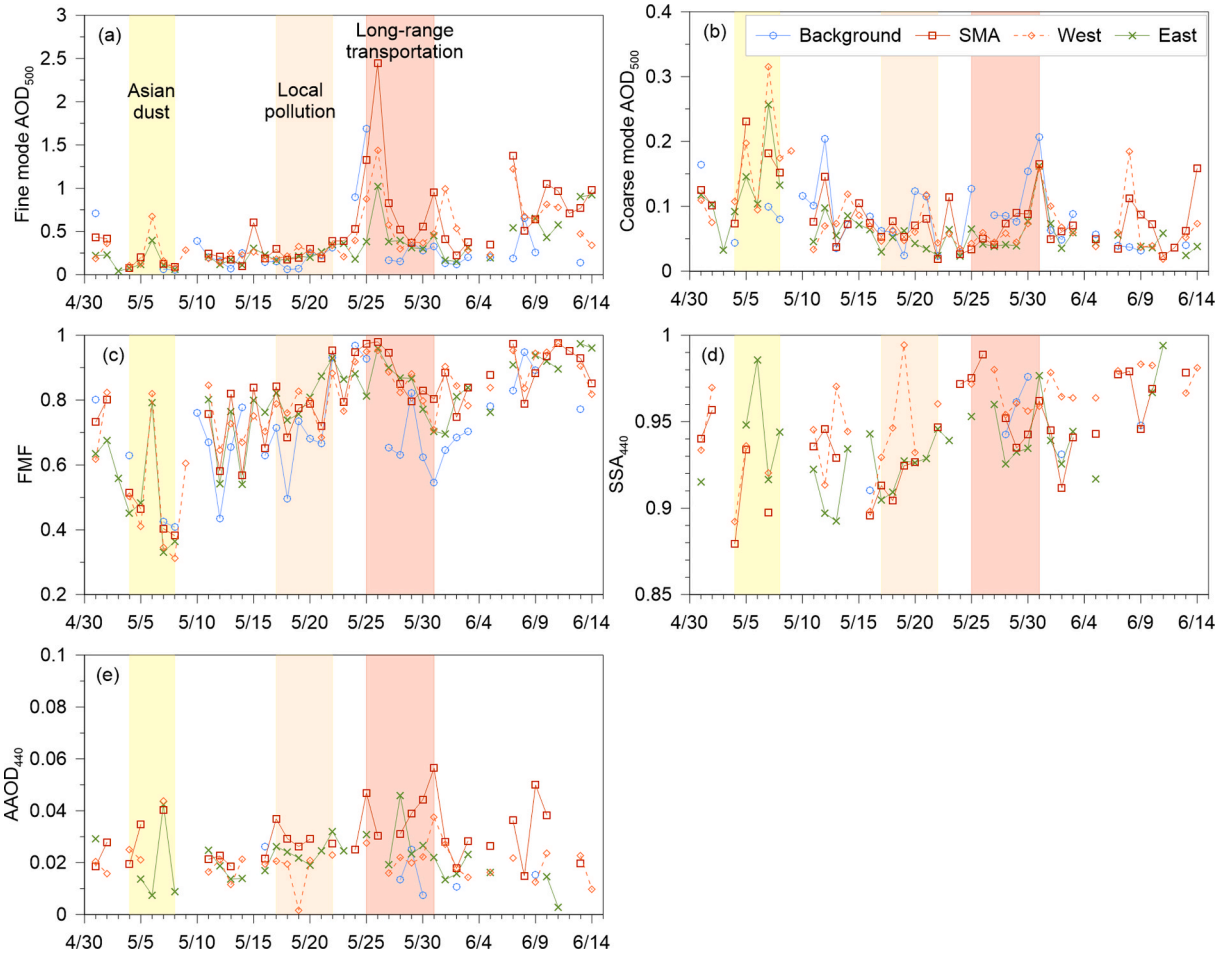

Fig. 5. Time series of daily average aerosol optical properties depending on AERONET clusters during the KORUS-AQ campaign. The shaded areas indicate high-aerosol loading episodes of Asian dust, local pollution, and long-range transportation, respectively.

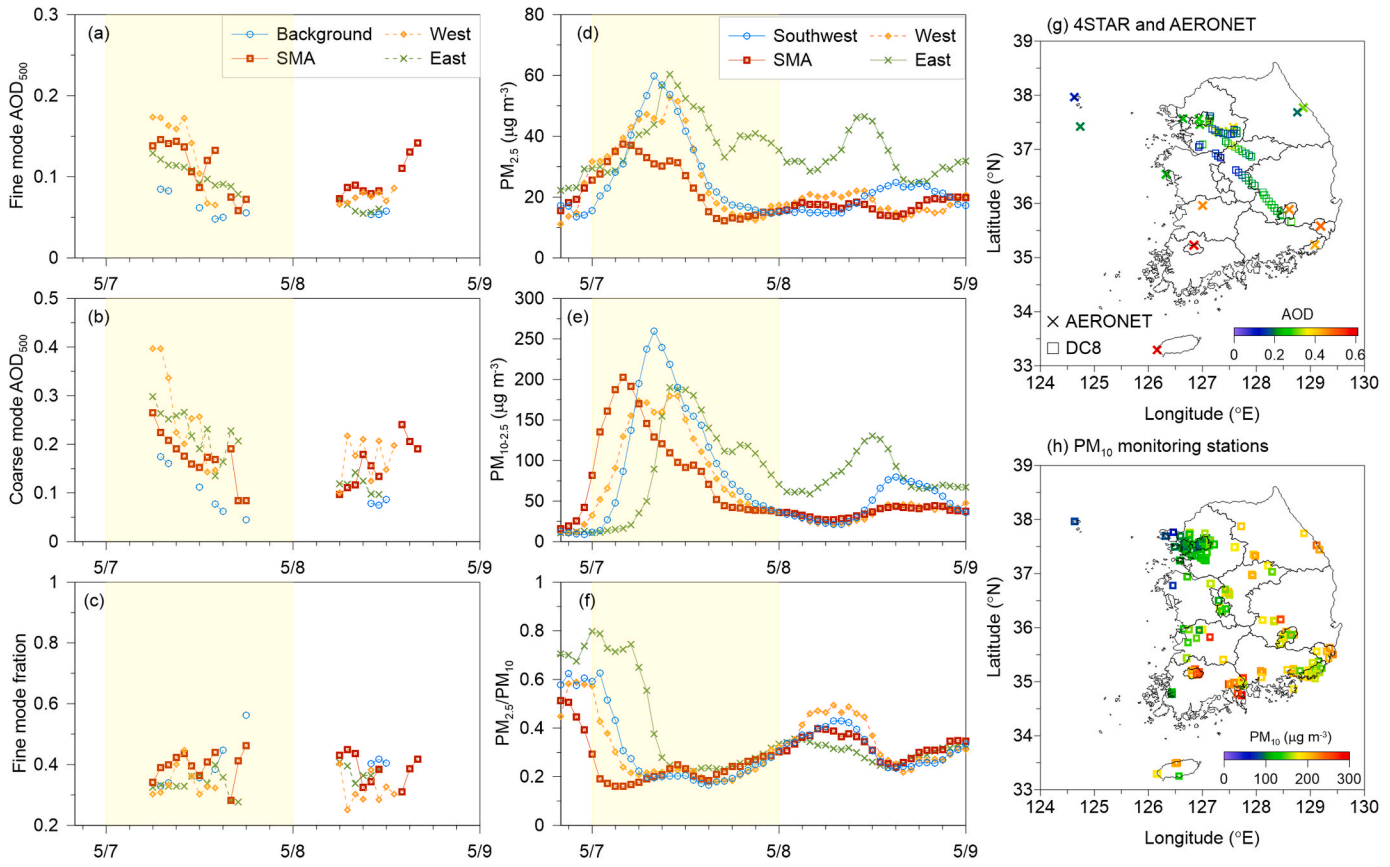

Fig. 6. Time series (a–f) of aerosol optical properties from AERONET and PM concentrations during the Asian dust episode (May 7) and spatial variation (g and h). (a) Fine-mode AOD, (b) coarse-mode AOD, (c) fine mode fraction (FMF) from AOD, (d) $PM_{2.5}$, (e) PM_{10}, and $PM_{2.5}/PM_{10}$, (g) AOD distribution from 4STAR (squares) and AERONET (crosses), and (h) PM10 distribution during the daytime when AOD could be measured. The shaded area indicates the day when the DC-8 research flight was conducted. The color of lines (a–f) and symbols (g–h) indicate correspondences to cluster and AOD (or PM_{10}), respectively. (For interpretation of the references to color in this figure legend, the reader is referred to the Web version of this article.)

As the effects of Asian dust diminished, local effects increased, especially on May 17, FMF and AAOD slightly increased with the local pollution. There were smaller temporal/spatial variations in fine-mode AOD, likely because of the increased concentration of BC and/or OC. However, the magnitude of the variation of fine-mode AOD was much lower than that of $PM_{2.5}$ (Fig. S2) because the planetary boundary layer might have been low. In contrast, fine-mode AOD was well captured the high $PM_{2.5}$ concentration during the long-range transportation on May 26, along with the high FMF and SSA indicating the dominance of anthropogenic pollutants, especially light-scattering aerosols such as ammonium nitrate and ammonium sulfate. The second highest peak was observed on May 31 along with the highest AAOD during the study period, suggesting a significant influence of Chinese pollution at the surface (Lamb et al., 2018).

Among the three cases of increased pollution (May 25, 30, and 31) that were also captured by the DC-8 flights, the events of May 25 and 31 showed that a highly polluted airmass was continuously advected from China to the western part of Korea, especially the Yellow Sea, which corresponded with high AOD in 4STAR (Fig. S4 and S5). On May 25, AERONET AOD gradually increased, with a high FMF (~1), until 17:00 LT, similar to $PM_{2.5}$ and $PM_{10\text{-}2.5}$ concentrations. These severe air quality conditions influenced a relatively broad area. AOD and PM_{10} were highest in the SMA and gradually decreased toward the south and/or east. May 30 to 31 had a mixed characteristic of stagnant conditions due to low wind speed and long-range transportation, similar to May 25, because there was no advected pollution across the Yellow Sea, as confirmed by 4STAR on May 30 (Fig. S5). AODs from AERONET and 4STAR in SMA on May 30 were much lower than those on May 31, although the $PM_{2.5}$ and $PM_{10\text{-}2.5}$ concentrations were similar on May 30 and 31, perhaps because of the passing of a large amount of aerosols above the planetary boundary layer on May 31, which the PM monitoring stations cannot measure. At noon on May 31, AOD, FMF, and $PM_{2.5}$ concentration in SMA rapidly decreased, but those variables in the western part of Korea simultaneously increased, especially in KORUS-Iksan in Jeollabuk-do. This feature was also captured by 4STAR AOD, which passed through those regions in the afternoon. However, the remainder of the western part of Korea (GIST and KORUS_Mokpo) did not show significant changes. Considering that $PM_{2.5}$ and O_3 concentrations were higher than in Seoul at that time, the photochemical reaction was more active in the afternoon. The distinct feature seen on May 30 and 31 was that AOD in the downwind of Seoul was higher than that in SMA, and both AOD and FMF increased from morning to afternoon (Fig. S5g and i). This could be explained by typical local effects, which are discussed in the next section.

3.4. Diurnal variation in the Seoul Metropolitan Area (SMA)

We used the missed approach flights over SMA during the KORUS-AQ campaign to investigate the diurnal variation in detail, because the flight path and the passing altitude were similar (Figs. 1b and 7a). The overall average AOD and AE from 4STAR during the missed approach was highest in Seoul, followed by the downwind and upwind regions (Fig. 7b and c). The AOD and AE in the downwind region were slightly higher than in the upwind region, because the downwind region was significantly influenced by pollutants transported from Seoul. The diurnal variation over SMA showed distinct characteristics, such as a

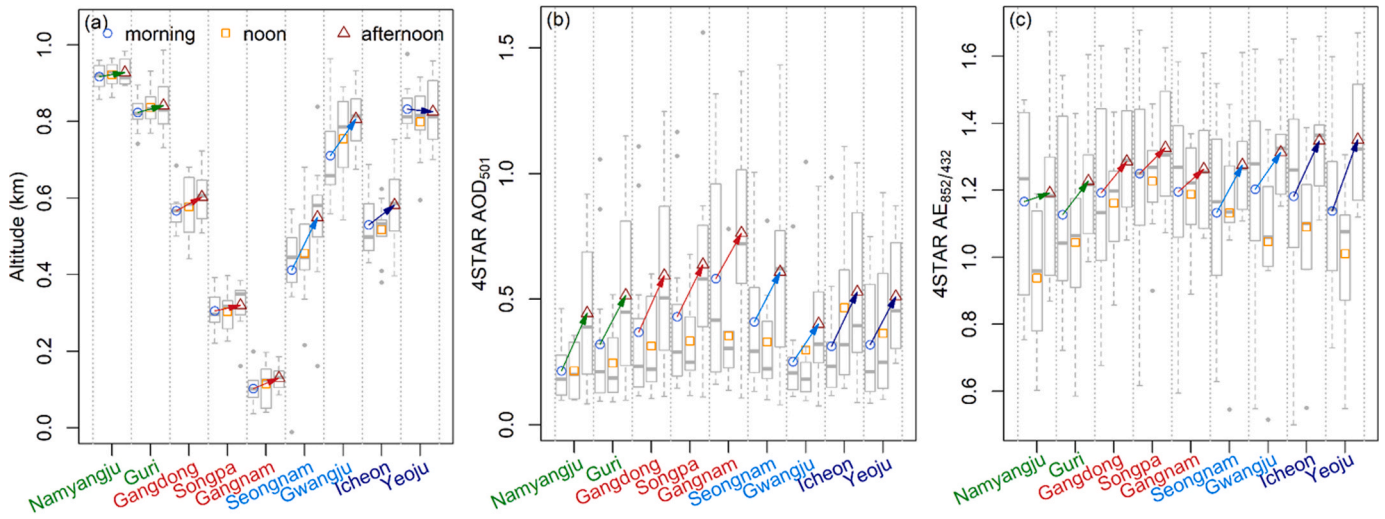

Fig. 7. The diurnal variation of DC-8 flight altitude, 4STAR AOD, and 4STAR AE over the SMA. The colored label in the *x*-axis and the arrows represent the upwind (green), Seoul (red), and downwind (blue) regions divided by administrative districts. The colored symbols indicate the corresponding DC-8 overpassing time (morning, noon, and afternoon). (For interpretation of the references to color in this figure legend, the reader is referred to the Web version of this article.)

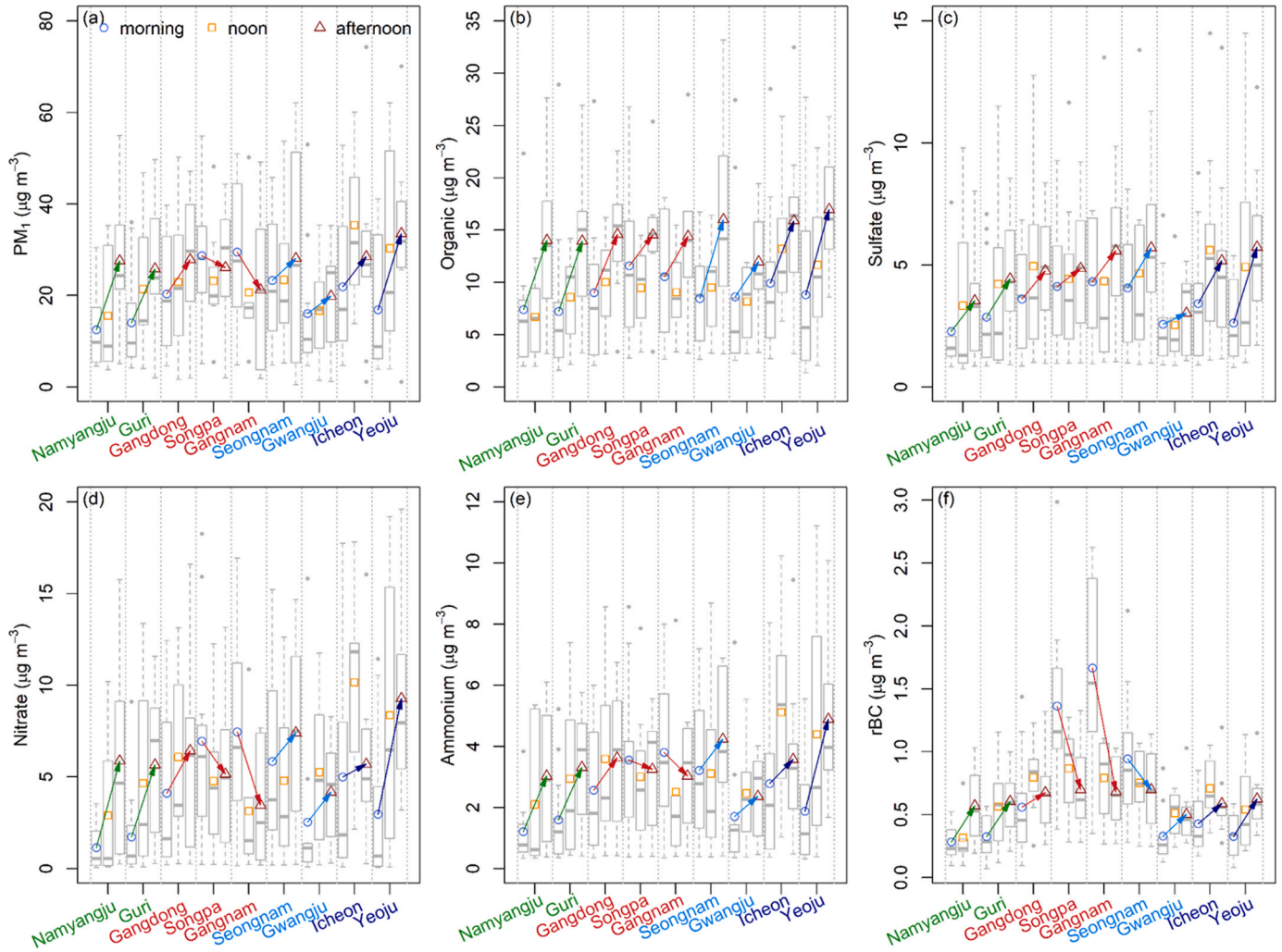

Fig. 8. Same as Fig. 7 except for PM_1 mass concentration and aerosol chemical components from high-resolution time-of-flight aerosol mass spectrometer (HR-ToF-AMS) and refractory black carbon (rBC) from Single Particle Soot Photometer (SP2). (a) PM_1, (b) organic, (c) sulfate, (d) nitrate, (e) ammonium, (f) rBC.

significant increase in AOD in the afternoon compared to the morning and noon, along with increasing AE. The increase of AOD in the early morning and evening according to traffic volume and gradually increasing AE were also observed in AERONET data, not only during the KORUS-AQ campaign but also in long-term data taken over the course of more than five years (Lennartson et al., 2018). The increasing magnitude of AE in the afternoon in the downwind region was more rapid than that in the upwind region and Seoul, but the magnitude of AOD was similar regardless of region. This result may imply more active secondary formation in the downwind region because of local pollutants and precursors for secondary formation (HNO_3 and H_2SO_4) advected from Seoul under ammonium-rich conditions.

When examining aerosol chemical composition in more detail, we noted similarities between the diurnal variation of fine-mode aerosol chemical composition and refractory BC (rBC) measured from high-resolution time-of-flight aerosol mass spectrometer (AMS) and single particle soot photometer (SP2), respectively (Fig. 8). Information on AMS and SP2, with which the DC-8 was equipped, was described in detail by Park et al. (2020), except for the pressure control inlet (Bahreini et al., 2008) and capture vaporizer (Hu et al., 2018), and Lamb et al. (2018), respectively. It should be noted that SP2 measured rBC with a volume equivalent diameter of 100–500 nm (assuming a void-free density of 1.8 g cm^{-3} for rBC), which quantified approximately 80–90% of rBC mass in the accumulation mode. The PM_1, which consisted of ammonium, sulfate, nitrate, organic aerosols, and rBC, showed a pattern similar to that of the AOD from 4STAR measurements except for Songpa and Gangnam, which are near the airport with missed-approached that have lower flight altitudes (less than 300 m). PM_1 concentration in the afternoon in the downwind region was much higher than that upwind and in Seoul, confirming an increase in secondary aerosol formation. Depending on the aerosol chemical composition, the concentrations of organic aerosols and sulfate in Seoul were increased from morning to afternoon, whereas ammonium, nitrate, and rBC showed a decreasing pattern along with PM_1 concentration, perhaps because of (1) a slight reduction in traffic volume of Seoul in the afternoon compared to morning (−7.1%) because NO_3, which is converted from NOx, and rBC emissions are mostly linked with transportation including gasoline and/or diesel vehicles and (2) a dilution in concentration because of increasing boundary layer height along with uplifting the rBC concentration at higher altitude (K. Lamb, personal communication, July 6, 2020). In addition, the decrease in ammonium nitrate concentration may be attributable to the dissociation of NH_4NO_3 because of favorable conditions for breakdown under higher temperature and lower relative humidity (Kim et al., 2015; Pathak et al., 2009). These distinct diurnal patterns of increasing temperature and decreasing relative humidity in Seoul were more remarkable than in the upwind and downwind regions (Fig. S5). However, columnar AOD was not affected by boundary layer height.

The highest organic aerosol (OA) concentration was observed in the downwind region, especially in Icheon and Yeoju, not Gwangju, which is located in the Taehwa forest, where there are high emissions of biogenic volatile organic compounds such as isoprene. Moreover, the OA concentration in the downwind region was steadily increased from morning to afternoon, but OA concentration in Seoul was lowest at noon. In general, isoprene is a well-known source of secondary OA (SOA) and its contribution to SOA formation is significant in rural regions (Henze and Seinfeld, 2006; Li et al., 2018; Shin et al., 2013). In addition, a large amount of isoprene is emitted from the forest during daylight hours because of a positive correlation with leaf temperature (Guenther et al., 1995, 1996). Considering that most OA in the downwind region were SOA (Nault et al., 2018), the concentrations of OA in Icheon and Yeoju were higher than that in Gwangju because of advection of isoprene from the forest and its photooxidation. In contrast, the decreasing OA in Seoul at noon, which led to reduction of PM_1 concentration, can be partially explained by the dominance of primary OA (mainly hydrocarbon-like OA and cooking OA) in this region, which also showed a rush-hour peak concentration in the early morning and minimum at noon (due to dilution of boundary layer) compared to high SOA at noon and/or afternoon (Kim et al., 2017, 2018). However, it is hard to interpret the increase in sulfate in the SMA with the decreasing RH (Fig. S6), because the major pathway of sulfate formation is in the aqueous phase, which mainly occurs in the clouds (Seinfeld and Pandis, 2016).

4. Summary and conclusions

By merging all available aerosol optical properties from AERONET, 4STAR on board the NASA DC-8, and PM concentration measurements from air quality monitoring stations over the Korean peninsula during the KORUS-AQ field campaign (April–June 2016), we investigated the temporal and spatial variations of aerosol optical properties including the detailed diurnal variation of aerosol chemical properties. Cluster analysis of the temporal variation of aerosol optical properties from AERONET data, using fine- and coarse-mode AOD and fine mode fraction (FMF), was applied by dividing the clusters into background, SMA, southwest, and east.

The average fine-mode AOD was highest in SMA, followed by southwest, east, and background, indicating a significant contribution of local pollutants and/or secondary formation near SMA rather than long-range transportation of aerosols. Moreover, the fine-mode AOD in the SMA gradually increased with distance from Seoul along with an increase in FMF and SSA in the downwind region. This can be explained by an increasing effect of light-scattering fine-mode aerosols due to secondary formation in the downwind region, whereas AAOD was highest at KORUS_Olympic_Park and Hankuk_UFS, indicating that carbonaceous aerosols were dominant. Coarse-mode AOD was much lower than fine-mode AOD and did not show any significant differences between clusters, because there was less effect of mineral dust during May and June according to meteorological conditions. The highest SSA with the lowest AOD was observed in KORUS-Daegwallyeong, which is located in a rural mountainous region (837 m asl) on the east coast of Korea, representing the dominance of maritime aerosols.

The R^2 for fine-mode AOD between AERONET sites at increasing distances showed higher values than those for coarse-mode AOD, along with a steeper slope of the linear least squares regression line (−0.16/100 km for fine-mode AOD and −0.14/100 km for coarse-mode AOD). It can be deduced that fine-mode aerosols were more spatially homogeneous than coarse-mode aerosols, because the fine-mode aerosols were usually transported on a regional scale rather than emitted from local emission sources. Moreover, the spatial distribution of aerosols in the west-to-east direction showed a more homogeneous characteristics compared to that in the north-to-south direction, because the long-range transported pollutants were moved by prevailing westerlies. However, the aerosol size distribution was more spatially homogeneous as the result of a consistent contribution of fine- and coarse-mode AOD to total AOD regardless of direction despite the higher spatial variability of fine-mode AOD.

According to the characteristics of high-aerosol loading episodes, the temporal and spatial variation of aerosol optical properties was well-matched with PM from air quality monitoring stations and 4STAR, providing detailed information on aerosol behavior and characteristics: a large effect of coarse-mode AOD ($PM_{10-2.5}$) during the Asian dust, the influence of carbonaceous aerosols during local pollution, and a significant contribution of fine-mode AOD ($PM_{2.5}$) during long-range transportation.

We investigated the detailed diurnal variation over the SMA using missed-approach flight segments with similar paths and altitudes. The diurnal variation over the SMA showed a significant increase in AOD in the afternoon compared to that in the morning and noon, along with increasing AE. Moreover, the magnitude of AE in the afternoon in the downwind region increased more rapidly than that in the upwind region and Seoul, because of more active secondary formation in the downwind region resulting from advected local pollutants and precursors for

secondary formation. This tendency generally agreed with the diurnal variation of PM_1 except in Songpa and Gangnam, suggesting a higher concentration in the downwind regions for these sites. The increase in PM_1 in the downwind regions may have resulted from an increase of secondary formation of SOA, ammonium nitrate, and ammonium sulfate. The increase in SOA and ammonium nitrate can be attributed to high concentrations of precursors (isoprene for SOA and NH_3 and HNO_3 for ammonium nitrate) with favorable meteorological conditions. However, the increasing ammonium sulfate along with decreasing RH is hard to interpret because the major formation pathway is an aqueous phase. Compared to the downwind region, ammonium nitrate and rBC were decreased in Songpa and Gangnam due to a reduction in traffic volume, dissociation of ammonium nitrate, and increase boundary layer height according to meteorological conditions in the afternoon.

Our results in this study provide detailed information on aerosol behavior gleaned from various measurement platforms, along with the evidence of active photochemical reactions in the downwind region. The results can be used to formulate policies to improve air quality in Korea, especially in the SMA region.

CRediT authorship contribution statement

Yongjoo Choi: Conceptualization, Methodology, Data curation, Writing – original draft, Writing – review & editing, Supervision. **Young Sung Ghim:** Writing – review & editing. **Michal Segal Rozenhaimer:** Writing – review & editing, Resources. **Jens Redemann:** Writing – review & editing. **Samuel E. LeBlanc:** Writing – review & editing. **Connor J. Flynn:** Resources. **Roy J. Johnson:** Resources. **Yonghwan Lee:** Resources. **Taehyoung Lee:** Resources. **Taehyun Park:** Resources. **Joshua P. Schwarz:** Writing – review & editing. **Kara D. Lamb:** Writing – review & editing, Resources. **Anne E. Perring:** Resources.

Declaration of competing interest

The authors declare that they have no known competing financial interests or personal relationships that could have appeared to influence the work reported in this paper.

Acknowledgments

This study was supported by National Research Foundation of Korea (NRF) grants funded by the Korea government (MSIT) (NRF-2018R1C1B6008004). We thank the National Institute of Environmental Research (NIER) for providing PM concentration through https://www.airkorea.or.kr/web/last_amb_hour_data?pMENU_NO=123 (in Korean). We thank all the AERONET principal investigators and their staff for establishing and maintaining the 20 AERONET sites used in this study. Finally, we acknowledge the DC-8 crews.

Appendix A. Supplementary data

Supplementary data to this article can be found online at https://doi.org/10.1016/j.atmosenv.2021.118301.

References

Al-Saadi, J., Kim, S., Song, C.-K., Chang, L.-S., Lee, G., Kim, J., Park, R., 2015. NASA Contributions to KORUS-AQ: an International Cooperative Air Quality Field Study in Korea. NASA.

Arola, A., Eck, T.F., Kokkola, H., Pitkänen, M.R.A., Romakkaniemi, S., 2017. Assessment of cloud-related fine-mode AOD enhancements based on AERONET SDA product. Atmos. Chem. Phys. 17, 5991–6001.

Arola, A., Schuster, G.L., Pitkänen, M.R.A., Dubovik, O., Kokkola, H., Lindfors, A.V., Mielonen, T., Raatikainen, T., Romakkaniemi, S., Tripathi, S.N., Lihavainen, H., 2015. Direct radiative effect by brown carbon over the Indo-Gangetic Plain. Atmos. Chem. Phys. 15, 12731–12740.

Bae, M.-S., Schauer, J.J., Lee, T., Jeong, J.-H., Kim, Y.-K., Ro, C.-U., Song, S.-K., Shon, Z.-H., 2017. Relationship between reactive oxygen species and water-soluble organic compounds: time-resolved benzene carboxylic acids measurement in the coastal area during the KORUS-AQ campaign. Environ. Pollut. 231, 1–12.

Bahreini, R., Dunlea, E.J., Matthew, B.M., Simons, C., Docherty, K.S., DeCarlo, P.F., Jimenez, J.L., Brock, C.A., Middlebrook, A.M., 2008. Design and operation of a pressure-controlled inlet for airborne sampling with an aerodynamic aerosol lens. Aerosol. Sci. Technol. 42, 465–471.

Cho, B., Song, M., 2017. Distributions and origins of PM10 in jeollabuk-do from 2010 to 2015. Journal of Korean Society for Atmospheric Environment 33, 251–264.

Choi, J., Park, R.J., Lee, H.-M., Lee, S., Jo, D.S., Jeong, J.I., Henze, D.K., Woo, J.-H., Ban, S.-J., Lee, M.-D., Lim, C.-S., Park, M.-K., Shin, H.J., Cho, S., Peterson, D., Song, C.-K., 2019a. Impacts of local vs. trans-boundary emissions from different sectors on PM2.5 exposure in South Korea during the KORUS-AQ campaign. Atmos. Environ. 203, 196–205.

Choi, M., Lim, H., Kim, J., Lee, S., Eck, T.F., Holben, B.N., Garay, M.J., Hyer, E.J., Saide, P.E., Liu, H., 2019b. Validation, comparison, and integration of GOCI, AHI, MODIS, MISR, and VIIRS aerosol optical depth over East Asia during the 2016 KORUS-AQ campaign. Atmos. Meas. Tech. 12, 4619–4641.

Choi, S.-H., Ghim, Y.S., Chang, Y.-S., Jung, K., 2014. Behavior of particulate matter during high concentration episodes in Seoul. Environ. Sci. Pollut. Control Ser. 21, 5972–5982.

Choi, Y., Ghim, Y.S., 2016. Estimation of columnar concentrations of absorbing and scattering fine-mode aerosol components using AERONET data. J. Geophys. Res. 121, 13628–13640.

Choi, Y., Ghim, Y.S., 2017. Assessment of the clear-sky bias issue using continuous PM10 data from two AERONET sites in Korea. J. Environ. Sci. 53, 151–160.

Choi, Y., Ghim, Y.S., Holben, B.N., 2016. Identification of columnar aerosol types under high aerosol optical depth conditions for a single AERONET site in Korea. J. Geophys. Res.: Atmosphere 121, 1264–1277.

Choi, Y., Ghim, Y.S., Zhang, Y., Park, S.-M., Song, I.-h., 2020. Estimation of surface concentrations of black carbon from long-term measurements at aeronet sites over Korea. Rem. Sens. 12, 3904.

Crippa, M., Guizzardi, D., Muntean, M., Schaaf, E., Dentener, F., van Aardenne, J.A., Monni, S., Doering, U., Olivier, J.G.J., Pagliari, V., Janssens-Maenhout, G., 2018. Gridded emissions of air pollutants for the period 1970–2012 within EDGAR v4.3.2. Earth Syst. Sci. Data 10, 1987–2013.

Dubovik, O., Sinyuk, A., Lapyonok, T., Holben, B.N., Mishchenko, M., Yang, P., Eck, T.F., Volten, H., Muñoz, O., Veihelmann, B., van der Zande, W.J., Leon, J.-F., Sorokin, M., Slutsker, I., 2006. Application of spheroid models to account for aerosol particle nonsphericity in remote sensing of desert dust. J. Geophys. Res. 111, D11208.

Dubovik, O., Smirnov, A., Holben, B.N., King, M.D., Kaufman, Y.J., Eck, T.F., Slutsker, I., 2000. Accuracy assessments of aerosol optical properties retrieved from Aerosol Robotic Network (AERONET) Sun and sky radiance measurements. J. Geophys. Res. 105, 9791–9806.

Dunagan, S., Johnson, R., Zavaleta, J., Russell, P., Schmid, B., Flynn, C., Redemann, J., Shinozuka, Y., Livingston, J., Segal-Rosenhaimer, M., 2013. Spectrometer for sky-scanning sun-tracking atmospheric research (4STAR): instrument technology. Rem. Sens. 5, 3872.

Eck, T.F., Holben, B.N., Reid, J.S., Dubovik, O., Smirnov, A., O'Neill, N.T., Slutsker, I., Kinne, S., 1999. Wavelength dependence of the optical depth of biomass burning, urban, and desert dust aerosols. J. Geophys. Res. 104, 31333–31349.

Ghim, Y.S., Choi, Y., Kim, S., Bae, C.H., Park, J., Shin, H.J., 2017. Evaluation of model performance for forecasting fine particle concentrations in Korea. Aerosol and Air Quality Research 17, 1856–1864.

Ghim, Y.S., Choi, Y., Park, J., Kim, S., Bae, C.H., Seo, J., Shin, H.J., Lim, Y.J., Lyu, Y.S., Lee, Y.J., 2019. Overall characteristics of nationwide high PM2.5 episodes during 2013~2016. Journal of Korean Society for Atmospheric Environment 35, 609–624.

Giles, D.M., Sinyuk, A., Sorokin, M.G., Schafer, J.S., Smirnov, A., Slutsker, I., Eck, T.F., Holben, B.N., Lewis, J.R., Campbell, J.R., Welton, E.J., Korkin, S.V., Lyapustin, A.I., 2019. Advancements in the Aerosol Robotic Network (AERONET) Version 3 database – automated near-real-time quality control algorithm with improved cloud screening for Sun photometer aerosol optical depth (AOD) measurements. Atmos. Meas. Tech. 12, 169–209.

Goldberg, D.L., Saide, P.E., Lamsal, L.N., de Foy, B., Lu, Z., Woo, J.H., Kim, Y., Kim, J., Gao, M., Carmichael, G., Streets, D.G., 2019. A top-down assessment using OMI NO2 suggests an underestimate in the NOx emissions inventory in Seoul, South Korea, during KORUS-AQ. Atmos. Chem. Phys. 19, 1801–1818.

Guenther, A., Hewitt, C.N., Erickson, D., Fall, R., Geron, C., Graedel, T., Harley, P., Klinger, L., Lerdau, M., Mckay, W.A., Pierce, T., Scholes, B., Steinbrecher, R., Tallamraju, R., Taylor, J., Zimmerman, P., 1995. A global model of natural volatile organic compound emissions. J. Geophys. Res.: Atmosphere 100, 8873–8892.

Guenther, A., Zimmerman, P., Klinger, L., Greenberg, J., Ennis, C., Davis, K., Pollock, W., Westberg, H., Allwine, G., Geron, C., 1996. Estimates of regional natural volatile organic compound fluxes from enclosure and ambient measurements. J. Geophys. Res.: Atmosphere 101, 1345–1359.

Ha, S., Liu, Z., Sun, W., Lee, Y., Chang, L., 2020. Improving air quality forecasting with the assimilation of GOCI aerosol optical depth (AOD) retrievals during the KORUS-AQ period. Atmos. Chem. Phys. 20, 6015–6036.

Henze, D.K., Seinfeld, J.H., 2006. Global secondary organic aerosol from isoprene oxidation. Geophys. Res. Lett. 33.

Holben, B.N., Eck, T.F., Slutsker, I., Tanré, D., Buis, J.P., Setzer, A., Vermote, E., Reagan, J.A., Kaufman, Y.J., Nakajima, T., Lavenu, F., Jankowiak, I., Smirnov, A., 1998. AERONET—a federated instrument network and data archive for aerosol characterization. Rem. Sens. Environ. 66, 1–16.

Holben, B.N., Kim, J., Sano, I., Mukai, S., Eck, T.F., Giles, D.M., Schafer, J.S., Sinyuk, A., Slutsker, I., Smirnov, A., Sorokin, M., Anderson, B.E., Che, H., Choi, M., Crawford, J. H., Ferrare, R.A., Garay, M.J., Jeong, U., Kim, M., Kim, W., Knox, N., Li, Z., Lim, H.S.,

Liu, Y., Maring, H., Nakata, M., Pickering, K.E., Piketh, S., Redemann, J., Reid, J.S., Salinas, S., Seo, S., Tan, F., Tripathi, S.N., Toon, O.B., Xiao, Q., 2018. An overview of mesoscale aerosol processes, comparisons, and validation studies from DRAGON networks. Atmos. Chem. Phys. 18, 655–671.

Holben, B.N., Tanré, D., Smirnov, A., Eck, T.F., Slutsker, I., Abuhassan, N., Newcomb, W. W., Schafer, J.S., Chatenet, B., Lavenu, F., Kaufman, Y.J., Castle, J.V., Setzer, A., Markham, B., Clark, D., Frouin, R., Halthore, R., Karneli, A., O'Neill, N.T., Pietras, C., Pinker, R.T., Voss, K., Zibordi, G., 2001. An emerging ground-based aerosol climatology: aerosol optical depth from AERONET. J. Geophys. Res. 106, 12067–12097.

Hu, W., Day, D.A., Campuzano-Jost, P., Nault, B.A., Park, T., Lee, T., Croteau, P., Canagaratna, M.R., Jayne, J.T., Worsnop, D.R., Jimenez, J.L., 2018. Evaluation of the new capture vaporizer for aerosol mass spectrometers: characterization of organic aerosol mass spectra. Aerosol. Sci. Technol. 52, 725–739.

Huang, M., Crawford, J.H., Diskin, G.S., Santanello, J.A., Kumar, S.V., Pusede, S.E., Parrington, M., Carmichael, G.R., 2018. Modeling regional pollution transport events during KORUS-AQ: progress and challenges in improving representation of land-atmosphere feedbacks. J. Geophys. Res.: Atmosphere 123 (10), 732-710,756.

Jeong, D., Seco, R., Gu, D., Lee, Y., Nault, B.A., Knote, C.J., McGee, T., Sullivan, J.T., Jimenez, J.L., Campuzano-Jost, P., Blake, D.R., Sanchez, D., Guenther, A.B., Tanner, D., Huey, L.G., Long, R., Anderson, B.E., Hall, S.R., Ullmann, K., Shin, H., Herndon, S.C., Lee, Y., Kim, D., Ahn, J., Kim, S., 2019. Integration of airborne and ground observations of nitryl chloride in the Seoul metropolitan area and the implications on regional oxidation capacity during KORUS-AQ 2016. Atmos. Chem. Phys. 19, 12779–12795.

Jordan, C.E., Crawford, J.H., Beyersdorf, A.J., Eck, T.F., Halliday, H.S., Nault, B.A., Chang, L.-S., Park, J., Park, R., Lee, G., Kim, H., Jun-young, A., Cho, S., Shin, H.J., Lee, J.H., Jung, J., Kim, D.-S., Lee, M., Lee, T., Whitehill, A., Szykman, J., Schueneman, M.K., Campuzano-Jost, P., Jimenez, J.L., DiGangi, J.P., Diskin, G.S., Anderson, B.E., Moore, R.H., Ziemba, L.D., Fenn, M.A., Hair, J.W., Kuehn, R.E., Holz, R.E., Chen, G., Travis, K., Shook, M., Peterson, D.A., Lamb, K.D., Schwarz, J.P., 2020. Investigation of factors controlling PM2.5 variability across the South Korean Peninsula during KORUS-AQ. Elem Sci Anth 8, 28. https://doi.org/10.1525/elementa.424.

Kim, C.H., Choi, Y., Ghim, Y.S., 2015. Characterization of volatilization of filter-sampled PM2.5 semi-volatile inorganic ions using a backup filter and denuders. Aerosol and Air Quality Research 15, 814–820.

Kim, H., Zhang, Q., Bae, G.N., Kim, J.Y., Lee, S.B., 2017. Sources and atmospheric processing of winter aerosols in Seoul, Korea: insights from real-time measurements using a high-resolution aerosol mass spectrometer. Atmos. Chem. Phys. 17, 2009–2033.

Kim, H., Zhang, Q., Heo, J., 2018. Influence of intense secondary aerosol formation and long-range transport on aerosol chemistry and properties in the Seoul Metropolitan Area during spring time: results from KORUS-AQ. Atmos. Chem. Phys. 18, 7149–7168.

Kim, S.-W., Yoon, S.-C., Jefferson, A., Ogren, J.A., Dutton, E.G., Won, J.-G., Ghim, Y.S., Lee, B.-I., Han, J.-S., 2005. Aerosol optical, chemical and physical properties at Gosan, Korea during Asian dust and pollution episodes in 2001. Atmos. Environ. 39, 39–50.

Kurokawa, J., Ohara, T., 2020. Long-term historical trends in air pollutant emissions in Asia: regional Emission inventory in ASia (REAS) version 3.1. Atmos. Chem. Phys. 20, 12761–12793. https://doi.org/10.5194/acp-20-12761-2020.

Lamb, K.D., Perring, A.E., Samset, B., Peterson, D., Davis, S., Anderson, B.E., Beyersdorf, A., Blake, D.R., Campuzano-Jost, P., Corr, C.A., Diskin, G.S., Kondo, Y., Moteki, N., Nault, B.A., Oh, J., Park, M., Pusede, S.E., Simpson, I.J., Thornhill, K.L., Wisthaler, A., Schwarz, J.P., 2018. Estimating source region influences on black carbon abundance, microphysics, and radiative effect observed over South Korea. J. Geophys. Res. Atmos. 123 (13), 527-513,548.

LeBlanc, S.E., Redemann, J., Flynn, C., Pistone, K., Kacenelenbogen, M., Segal-Rosenheimer, M., Shinozuka, Y., Dunagan, S., Dahlgren, R.P., Meyer, K., Podolske, J., Howell, S.G., Freitag, S., Small-Griswold, J., Holben, B., Diamond, M., Wood, R., Formenti, P., Piketh, S., Maggs-Kölling, G., Gerber, M., Namwoonde, A., 2020. Above-cloud aerosol optical depth from airborne observations in the southeast Atlantic. Atmos. Chem. Phys. 20, 1565–1590.

Lee, H.J., Son, Y.-S., 2016. Spatial variability of AERONET aerosol optical properties and satellite data in South Korea during NASA DRAGON-asia campaign. Environ. Sci. Technol. 50, 3954–3964.

Lee, Y.H., Choi, Y., Ghim, Y.S., 2016. Classification of diurnal patterns of particulate inorganic ions downwind of metropolitan Seoul. Environ. Sci. Pollut. Res. 23, 8917–8928.

Lennartson, E.M., Wang, J., Gu, J., Castro Garcia, L., Ge, C., Gao, M., Choi, M., Saide, P. E., Carmichael, G.R., Kim, J., Janz, S.J., 2018. Diurnal variation of aerosol optical depth and PM2.5 in South Korea: a synthesis from AERONET, satellite (GOCI), KORUS-AQ observation, and the WRF-Chem model. Atmos. Chem. Phys. 18, 15125–15144.

Li, J., Wang, G., Wu, C., Cao, C., Ren, Y., Wang, J., Li, J., Cao, J., Zeng, L., Zhu, T., 2018. Characterization of isoprene-derived secondary organic aerosols at a rural site in North China Plain with implications for anthropogenic pollution effects. Sci. Rep. 8, 535.

Li, Z., Zhang, Y., Xu, H., Li, K., Dubovik, O., Goloub, P., 2019. The fundamental aerosol models over China region: a cluster Analysis of the ground-based remote sensing measurements of total columnar atmosphere. Geophys. Res. Lett. 46, 4924–4932.

Linke, C., Möhler, O., Veres, A., Mohácsi, Á., Bozóki, Z., Szabó, G., Schnaiter, M., 2006. Optical properties and mineralogical composition of different Saharan mineral dust samples: a laboratory study. Atmos. Chem. Phys. 6, 3315–3323.

Miyazaki, K., Sekiya, T., Fu, D., Bowman, K.W., Kulawik, S.S., Sudo, K., Walker, T., Kanaya, Y., Takigawa, M., Ogochi, K., Eskes, H., Boersma, K.F., Thompson, A.M., Gaubert, B., Barre, J., Emmons, L.K., 2019. Balance of emission and dynamical controls on ozone during the Korea-United States air quality campaign from multiconstituent satellite data assimilation. J. Geophys. Res.: Atmosphere 124, 387–413.

Myhre, G., Shindell, D., Bréon, F., Collins, W., Fuglestvedt, J., Huang, J., Koch, D., Lamarque, J., Lee, D., Mendoza, B., 2013. Anthropogenic and natural radiative forcing. Climate change 423.

Nault, B.A., Campuzano-Jost, P., Day, D.A., Schroder, J.C., Anderson, B., Beyersdorf, A. J., Blake, D.R., Brune, W.H., Choi, Y., Corr, C.A., de Gouw, J.A., Dibb, J., DiGangi, J. P., Diskin, G.S., Fried, A., Huey, L.G., Kim, M.J., Knote, C.J., Lamb, K.D., Lee, T., Park, T., Pusede, S.E., Scheuer, E., Thornhill, K.L., Woo, J.H., Jimenez, J.L., 2018. Secondary organic aerosol production from local emissions dominates the organic aerosol budget over Seoul, South Korea, during KORUS-AQ. Atmos. Chem. Phys. 18, 17769–17800.

O'Neill, N.T., Eck, T.F., Holben, B.N., Smirnov, A., Dubovik, O., Royer, A., 2001. Bimodal size distribution influences on the variation of Angstrom derivatives in spectral and optical depth space. J. Geophys. Res.: Atmosphere 106, 9787–9806.

O'Neill, N.T., Eck, T.F., Smirnov, A., Holben, B.N., Thulasiraman, S., 2003. Spectral discrimination of coarse and fine mode optical depth. J. Geophys. Res.: Atmosphere 108 (n/a-n/a).

Park, S., Yu, G.-H., Lee, S., 2018. Optical absorption characteristics of brown carbon aerosols during the KORUS-AQ campaign at an urban site. Atmos. Res. 203, 16–27.

Park, T., Choi, Y., Choi, J., Ahn, J., Park, J., Lee, Y., Ban, J., Park, G., Kang, S., Kim, K., Seo, B.-K., Kim, J., Park, S., Kim, H., Jeon, H., Lee, T., 2020. Aircraft measurements of physicochemical evolution of atmospheric aerosols in air pollution plumes over a megacity and suburban areas. Aerosol and Air Quality Research 20.

Pathak, R.K., Wu, W.S., Wang, T., 2009. Summertime PM2.5 ionic species in four major cities of China: nitrate formation in an ammonia-deficient atmosphere. Atmos. Chem. Phys. 9, 1711–1722.

Peterson, D.A., Hyer, E.J., Han, S.-O., Crawford, J.H., Park, R.J., Holz, R., Kuehn, R.E., Eloranta, E., Knote, C., Jordan, C.E., 2019. Meteorology influencing springtime air quality, pollution transport, and visibility in Korea. Elem Sci Anth 7, 57.

Pope, C.A., Dockery, D.W., 2006. Health effects of fine particulate air pollution: lines that connect. J. Air Waste Manag. Assoc. 56, 709–742.

Prats, N., Cachorro, V.E., Berjón, A., Toledano, C., De Frutos, A.M., 2011. Column-integrated aerosol microphysical properties from AERONET Sun photometer over southwestern Spain. Atmos. Chem. Phys. 11, 12535–12547.

Quinn, P.K., Bates, T.S., 2005. Regional aerosol properties: comparisons of boundary layer measurements from ACE 1, ACE 2, Aerosols99, INDOEX, ACE Asia, TARFOX, and NEAQS. J. Geophys. Res.: Atmosphere 110 (n/a-n/a).

Russell, P.B., Kacenelenbogen, M., Livingston, J.M., Hasekamp, O.P., Burton, S.P., Schuster, G.L., Johnson, M.S., Knobelspiesse, K.D., Redemann, J., Ramachandran, S., 2014. A multiparameter aerosol classification method and its application to retrievals from spaceborne polarimetry. J. Geophys. Res.: Atmosphere 119, 9838–9863.

Sayer, A.M., Hsu, N.C., Lee, J., Kim, W.V., Burton, S., Fenn, M.A., Ferrare, R.A., Kacenelenbogen, M., LeBlanc, S., Pistone, K., Redemann, J., Segal-Rozenhaimer, M., Shinozuka, Y., Tsay, S.C., 2019. Two decades observing smoke above clouds in the south-eastern Atlantic Ocean: deep Blue algorithm updates and validation with ORACLES field campaign data. Atmos. Meas. Tech. 12, 3595–3627.

Schuster, G.L., Dubovik, O., Arola, A., 2016a. Remote sensing of soot carbon – Part 1: distinguishing different absorbing aerosol species. Atmos. Chem. Phys. 16, 1565–1585.

Schuster, G.L., Dubovik, O., Arola, A., Eck, T.F., Holben, B.N., 2016b. Remote sensing of soot carbon – Part 2: understanding the absorption Ångström exponent. Atmos. Chem. Phys. 16, 1587–1602.

Schuster, G.L., Dubovik, O., Holben, B.N., 2006. Angstrom exponent and bimodal aerosol size distributions. J. Geophys. Res. 111, D07207.

Segal-Rosenheimer, M., Russell, P.B., Livingston, J.M., Ramachandran, S., Redemann, J., Baum, B.A., 2013. Retrieval of cirrus properties by Sun photometry: a new perspective on an old issue. J. Geophys. Res.: Atmosphere 118, 4503–4520.

Segal-Rosenheimer, M., Russell, P.B., Schmid, B., Redemann, J., Livingston, J.M., Flynn, C.J., Johnson, R.R., Dunagan, S.E., Shinozuka, Y., Herman, J., Cede, A., Abuhassan, N., Comstock, J.M., Hubbe, J.M., Zelenyuk, A., Wilson, J., 2014. Tracking elevated pollution layers with a newly developed hyperspectral Sun/Sky spectrometer (4STAR): results from the TCAP 2012 and 2013 campaigns. J. Geophys. Res.: Atmosphere 119, 2611–2628.

Seinfeld, J.H., Pandis, S.N., 2016. Atmospheric Chemistry and Physics: from Air Pollution to Climate Change. John Wiley & Sons.

Shin, H.J., Kim, J.C., Lee, S.J., Kim, Y.P., 2013. Evaluation of the optimum volatile organic compounds control strategy considering the formation of ozone and secondary organic aerosol in Seoul, Korea. Environ. Sci. Pollut. Control Ser. 20, 1468–1481.

Shinozuka, Y., Johnson, R.R., Flynn, C.J., Russell, P.B., Schmid, B., Redemann, J., Dunagan, S.E., Kluzek, C.D., Hubbe, J.M., Segal-Rosenheimer, M., Livingston, J.M., Eck, T.F., Wagener, R., Gregory, L., Chand, D., Berg, L.K., Rogers, R.R., Ferrare, R.A., Hair, J.W., Hostetler, C.A., Burton, S.P., 2013. Hyperspectral aerosol optical depths from TCAP flights. J. Geophys. Res.: Atmosphere 118 (12), 180-112,194.

Sinyuk, A., Holben, B.N., Eck, T.F., Giles, D.M., Slutsker, I., Korkin, S., Schafer, J.S., Smirnov, A., Sorokin, M., Lyapustin, A., 2020. The AERONET Version 3 aerosol retrieval algorithm, associated uncertainties and comparisons to Version 2. Atmos. Meas. Tech. Discuss. 2020, 1–80.

Smirnov, A., Holben, B.N., Giles, D.M., Slutsker, I., O'Neill, N.T., Eck, T.F., Macke, A., Croot, P., Courcoux, Y., Sakerin, S.M., Smyth, T.J., Zielinski, T., Zibordi, G., Goes, J.

I., Harvey, M.J., Quinn, P.K., Nelson, N.B., Radionov, V.F., Duarte, C.M., Losno, R., Sciare, J., Voss, K.J., Kinne, S., Nalli, N.R., Joseph, E., Krishna Moorthy, K., Covert, D.S., Gulev, S.K., Milinevsky, G., Larouche, P., Belanger, S., Horne, E., Chin, M., Remer, L.A., Kahn, R.A., Reid, J.S., Schulz, M., Heald, C.L., Zhang, J., Lapina, K., Kleidman, R.G., Griesfeller, J., Gaitley, B.J., Tan, Q., Diehl, T.L., 2011. Maritime aerosol network as a component of AERONET – first results and comparison with global aerosol models and satellite retrievals. Atmos. Meas. Tech. 4, 583–597.

Smirnov, A., Holben, B.N., Kaufman, Y.J., Dubovik, O., Eck, T.F., Slutsker, I., Pietras, C., Halthore, R.N., 2002. Optical properties of atmospheric aerosol in maritime environments. J. Atmos. Sci. 59, 501–523.

WHO, 2006. Health Risks of Particulate Matter from Long-Range Transboundary Air Pollution. WHO Regional Office for Europe, Copenhagen, Denmark.

Zhang, Y., Li, Z., Sun, Y., Lv, Y., Xie, Y., 2018. Estimation of atmospheric columnar organic matter (OM) mass concentration from remote sensing measurements of aerosol spectral refractive indices. Atmos. Environ. 179, 107–117.

Zheng, B., Tong, D., Li, M., Liu, F., Hong, C., Geng, G., Li, H., Li, X., Peng, L., Qi, J., Yan, L., Zhang, Y., Zhao, H., Zheng, Y., He, K., Zhang, Q., 2018. Trends in China's anthropogenic emissions since 2010 as the consequence of clean air actions. Atmos. Chem. Phys. 18, 14095–14111.